J. Raman Spectroscopy, **27**, 579-586 (1996)

Invited Contribution to

JOURNAL OF RAMAN SPECTROSCOPY

"RAMAN MICROSCOPY AND IMAGING"

Nano-Raman Spectroscopy and Imaging with the Near-field Scanning Optical Microscope

[1] C.L. Jahncke, H.D. Hallen, and *M.A. Paesler
Physics Department, North Carolina State University
Raleigh, NC 27695-8202

Abstract

We have performed Raman spectroscopy using a near-field scanning optical microscope. This avoids the diffraction limit inherent with conventional optical microscopy techniques involving far-field optical components, and allows volumes significantly smaller than the cube of the wavelength to be investigated. The small sample volume coupled with the light-starved nature of the Raman effect itself makes such nano-Raman studies difficult. We describe a near-field Raman microscope and present results showing near-field effects in an investigation of Rb-doped KTP. An image taken within a Raman feature demonstrates that nano-Raman imaging is indeed possible if the near-field instrument has considerable long-term stability, and that several unique aspects of the near field data recommend this approach.

I. Introduction

Optical microscopy and Raman spectroscopy are proven analytical tools that have been successfully coupled in micro-Raman studies that span a broad range of materials and applications. By their very natures, however, the two techniques each independently contribute to severe restrictions in the amount of light available for analysis and imaging. Microscopy gathers light from a restricted sample volume, and Raman spectroscopy involves use of a restricted spectral band of light involving an effect with relatively low quantum efficiency. The consequent light-starved nature of micro-Raman spectroscopy can make advances toward finer spatial or spectral resolution difficult.

---

[1] Current address: Physics Department, St. Lawrence University, Canton, NY 13617

The near-field scanning optical microscope, or NSOM, allows one to optically study regions near the surface of a sample that can be significantly smaller than the wavelength of the probe radiation. The NSOM surpasses the diffraction limit imposed on far-field devices by the scanning of a sub-wavelength aperture across the near-field above the surface of a sample. We have coupled an NSOM to a Raman spectrometer to demonstrate that one can perform *nano*-Raman spectroscopy.

In the following we first describe the general nature of near-field imaging and spectroscopy. Then we outline the design considerations necessary to allow one to maintain the stability necessary for sub-wavelength scanning and imaging precision over time scales sufficient to collect meaningful Raman scattered light from nanoscopic regions of a sample. Raman spectra of Rb-doped KTP are presented as demonstrations of nano-Raman spectroscopy, and we provide an NSOM image taken within a Raman line. Finally, we discuss features of spectra that are particular to an NSOM investigation. We note surface sensitivity, polarization effects, and a reduced Rayleigh tail in addition to the resolution of NSOM and the fact that NSOM provides a simultaneous topographic image of the region under investigation.

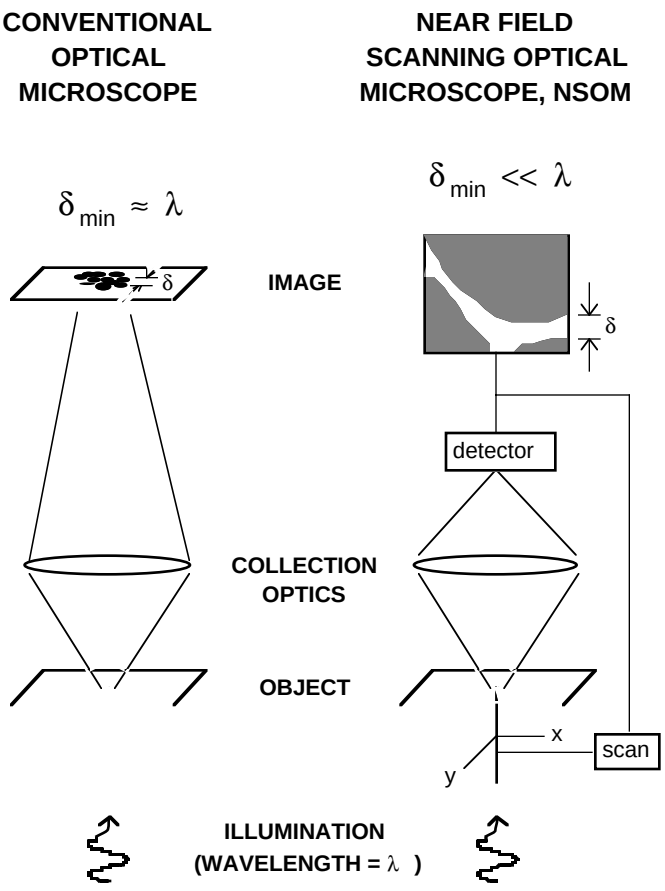

Figure 1. Schematic representation of a conventional and a scanning near-field optical microscope. In both instruments, illumination of wavelength λ is incident from below.

II. The Near-field Scanning Optical Microscope, or NSOM

When one uses a conventional optical microscope to image, the smallest resolvable objects can be only slightly smaller than the wavelength λ of the light used to image them. This resolution limit - the so-called Abbe barrier - is a fundamental consequence of the diffraction of light when conventional far-field devices are used to image. With an NSOM, resolution well past the Abbe barrier is possible, and new vistas are available to the

analytical microscopist. This dramatically enhanced resolution is obtained by confining the optical fields in the vicinity of a sample to sub-λ dimensions.

An NSOM resembles a scanning tunneling microscope with the conducting needle-like probe replaced with a tapered optical fiber that has been coated with a reflecting film. The instrument is compared schematically to a conventional far-field microscope in figure 1. In both instruments, a sample is illuminated from below. In the conventional microscope, light is collected by a lens and features of the sample appear in an image plane. In an ideal conventional optical microscope, the smallest feature that can be resolved is on the order of $\lambda/2$. In the NSOM shown schematically on the right of figure 1, the optical field passing through a tapered fiber is confined to nanometric dimensions by a sub-λ sized aperture at the apex of the taper. By scanning the aperture across the sample surface in its optical near-field, information can be gathered and processed in a computer to reveal an image of the surface of the sample with nanometric precision. The NSOM has in recent years established itself as a powerful laboratory analytical tool. Documentation of its capabilities can be found in a number of sources including original research contributions,[1-3] conference proceedings,[4] and texts.[5]

If an NSOM aperture is simply scanned across a sample in a plane, image interpretation can be complicated by the mixing of topographic and optical information. That is, a change in signal from one position on the sample to the next could be indicative of a change in sample topography or optical density. To reduce this confusion, the NSOM is typically operated in a shear-force feedback mode. In this mode, the aperture follows a sample's topographic contours while scanning so as to obtain an image of the optical signal where the probe is typically ~10 nm above the surface. Such operation has the additional advantage of yielding an independent shear-force topographic image that can be quite useful in interpreting the optical data. In this mode of operation, the shear force between the optical fiber probe and the surface of the sample is sensed by dithering the taper laterally a few nanometers while scanning. Measurement of the damping of the amplitude of the dithering allows one to determine the sample-tip shear force and thus sample topography.

The NSOM has many of the advantages of conventional optical microscopy without the resolution limit inherent in far-field imaging. In particular, one has a wealth of contrast mechanisms at one's disposal. For example, information about the sample can be gleaned from the optical signal's intensity, polarization state, temporal behavior, or spectral content. Other advantages of the NSOM include the non-invasive nature of an optical probe, the ability to work in a wide variety of environments, the

simultaneous topographic images, and the relative lack of any unusual sample preparation procedures. The disadvantages have been noted above: the area to be imaged must be close (less than the aperture size) to the probe or resolution is affected, and signal level is reduced by the small sample volume inherent to high spatial resolution and by the coupling of light through the probe.

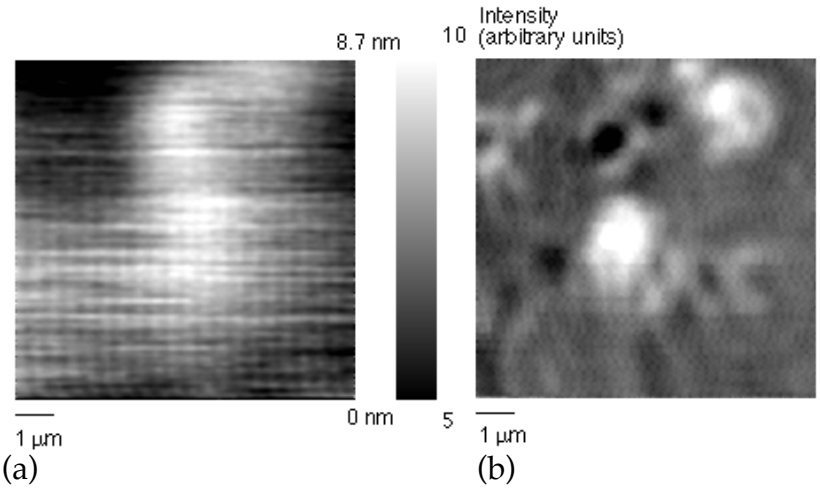

Figure 2. Simultaneously acquired a) topographic and b) NSOM transmission images of a 9 μm square region of a sample upon which particulates have been impacted. Several featureless particulates are seen in the topography (which varies over 18 nm), while the internal details are observed in the optical image.

As an example of NSOM imaging, we present in figure 2 images of particulates collected from the air by impaction onto a sapphire substrate. Each of these images is 9 μm square. The topography of the particulates is presented in figure 2(a) with a vertical range of 18 nm It provides little information about the internal structure of the particulates. The NSOM optical image, figure 2(b), taken in transmission with green (514.5 nm) light, reveals the details of the internal structure.

In the work presented here, it is of course the spectral information in the optical signal that is of interest. With its dramatically smaller quantum efficiency Raman spectroscopy provides a much stiffer challenge to the near-field microscopist. Some preliminary work suggested sufficient signal could be collected through an NSOM probe to take a Raman spectrum.[6] Early studies, however, involved such low counting rates that the spectra-gathering times were too long to insure nano-scopic spatial resolution. Quite simply, instrument drift over the many hours required rendered the spatial resolution moot. Other Raman data obtained in the near-field were taken with an uncoated probe and no scanning was demonstrated.[7]

III. Experiment

Figure 3 is a schematic of the experimental setup. A cooled photomultiplier tube in the photon counting mode is used in conjunction

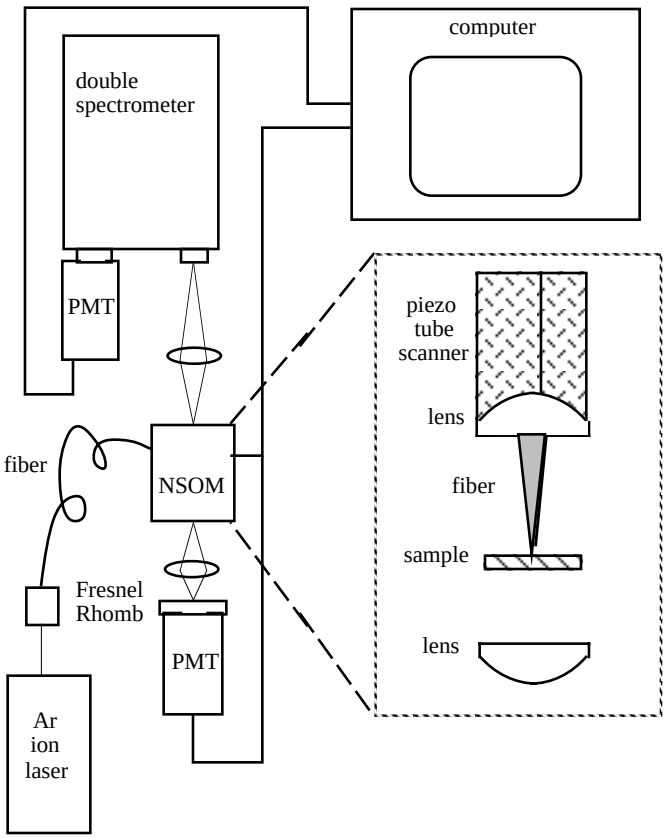

Figure 3. Schematic of the experimental Raman set-up with the NSOM shown in the inset.

with a SPEX Czerney-Turner double spectrometer for the Raman signal detection. The slits on the spectrometer were all set to 400 μm corresponding to a 4 cm^{-1} resolution. An Argon Ion laser tuned to 514.5 nm provides the excitation source. The laser light is directed through an interference filter to remove plasma lines. A Fresnel Rhomb and/or waveplates can be used to rotate the polarization of the light before coupling it into the probe tip which is mounted in the NSOM.

The NSOM probes are Al coated tapered optical fibers. The tapers are made by a commonly used heating and pulling technique. In a commercial instrument most commonly used for micro-pipette manufacture, an optical fiber is placed under tensile stress and locally heated with a CO_2 laser. When softening is sensed, the tension is increased and the laser is extinguished. The subsequent fracture results in a fiber tapered to a flat cleave at the end, as small as ten nanometers across. Taper shape and size can be controlled by adjusting pulling parameters such as the laser power, the two tensions and the delay between softening and increasing of the tension. An aperture is placed on the tapers by evaporating an Al coating over the taper as it rotates. By directing the axis of rotation slightly out of the evaporant stream one can create an aperture diameter on the apex of the taper as small 10^{-8} m.

Perhaps the most distinct feature of the NSOM designed for these Raman studies is its ultra stable construction. Since Raman spectra collection times of many hours were anticipated, the instrument was designed to maintain its position to within the desired precision for times this long. This was accomplished by a combination of symmetry, compact design and thermal isolation. The NSOM, described in detail elsewhere[8] measures less than four inches long by 1.75 inches in width. The probe tip is symmetrically mounted within a lens used for collecting reflected light, while a similar lens collects transmitted light simultaneously. This is shown in the inset of figure

3, and permits the simultaneous detection of topography, Raman in reflection, and an NSOM intensity image in transmission. Coarse positioning utilized piezo-electric elements driving the probe with a stick-slip motion. The entire microscope was enclosed in a thermally-insulated metal container during operation. The sample is illuminated through the probe which is mounted into a 0.55 N.A. aspheric lens. The backscattered light from the sample is collected with this lens and then focused into the spectrometer.

Potassium titanyl phosphate (KTP) is the sample we chose for our near-field Raman investigations. It is a nonlinear optical material primarily used for frequency doubling applications. The KTP crystal was selected for two reasons. First, it has a strong Raman signal making it a good candidate for Raman signal detection. Secondly, our particular sample contained regions doped with rubidium which should differ spectrally and spatially from the bulk KTP. In imaging this crystal we expect to be able to study how the sample's spectroscopic signal might vary spatially.

KTP is an orthorhombic crystal belonging to the C_{2v} point group and the $Pna2_1$ - C_{2v}^9 space group. KTP contains 8 molecules per primitive unit cell. The lattice constants are a = 12.814 Å, b = 6.404 Å and c = 10.616 Å. The crystal is comprised of chains of TiO_6 octahedra which are linked at two corners and separated by PO_4 tetrahedra. There are two chains per unit cell, and their direction alternates between (011) and $(0\bar{1}\ 1)$. The Ti-O bonds which occur along these chains alternate between long and short bonds resulting in a net z polarization. The K ion is weakly bonded to both the Ti octahedra and the P tetrahedra. The large nonlinear optic and electro-optic coefficients are primarily due to the alternating long and short Ti-O bonds. There are channels which exist along the z-direction allowing for a diffusion coefficient of K atoms (or similar atoms) that is several orders of magnitude larger in the z-direction than the x or y direction.[9]

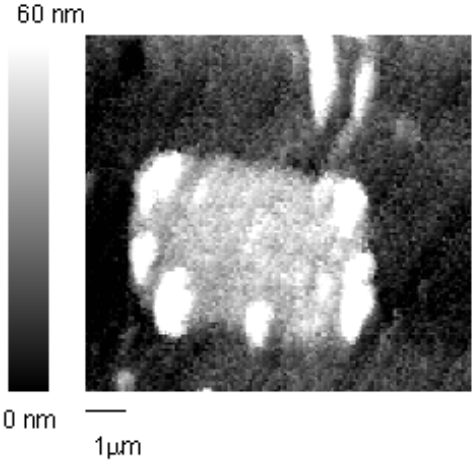

Figure 4. A 10 μm square shear-force image of the KTP surface. The light spot in the center is the Rb-doped region. The doped region is approximately 12 nm higher than the background undoped bulk KTP.

The difference between the diffusion coefficient in the z-direction and the x-y plane enables the sample to be doped with materials such as Rb in a waveguide fashion.[10, 11] The sample we used contains an array of 5 micron

square regions doped with rubidium through potassium ion exchange during diffusion, thus forming rubidium titanyl phosphate (RTP) areas. Doping results in a change in the refractive index, so that surface waveguides can be fabricated. A result of this process is a slight expansion of the KTP matrix which manifests itself in regions that are raised approximately 12 nm above the bulk KTP. Figure 4 shows a 10 micron square shear force scan of the KTP surface where the light area in the center is a typical Rb doped region. Before examining the Raman spectrum of this sample, we refer briefly to its point group symmetries.

The C_{2v} point group has A1, A2, B1, and B2 symmetries and the optical vibration modes are

$$\Gamma = 47\ A1 + 48\ A2 + 47\ B1 + 47\ B2$$

for a total of 189. All of these vibrations are Raman active, and the Raman tensors for these symmetries are

$$A1 = \begin{bmatrix} \alpha_{xx} & & \\ & \alpha_{yy} & \\ & & \alpha_{zz} \end{bmatrix}, \qquad A2 = \begin{bmatrix} & \alpha_{xy} & \\ \alpha_{yx} & & \\ & & \end{bmatrix},$$

$$B1 = \begin{bmatrix} & & \alpha_{xz} \\ & & \\ \alpha_{zx} & & \end{bmatrix}, \text{ and } B2 = \begin{bmatrix} & & \\ & & \alpha_{yz} \\ & \alpha_{zy} & \end{bmatrix}$$

The important point to make here is that it is possible to examine the vibration types, A1, B1, A2, and B2, independantly by using different polarization geometries. Several such studies have been completed[12, 13]. In our experiment, we will examine the crystal in the backscattering direction $(00\bar{1})$. The Raman scattering geometry is $z(xyxy)\bar{z}$. That is, the incident light is unpolarized light propagating in the z-direction, and the scattered light was collected without an analyzer in the -z direction. With this type of geometry, only the A1 and the A2 vibrational modes should be observed.

IV. Near-field Raman Spectra and Images

The Raman spectrum in the KTP region should differ from the RTP waveguide region due to the induced stress as well as the mass difference between K and Rb. Near-field Raman spectra from each region are shown in figure 5. The strongest feature in each spectrum is at 767 cm^{-1}. This is an A1 vibrational mode and peaks in this region have been assigned to the TiO_6

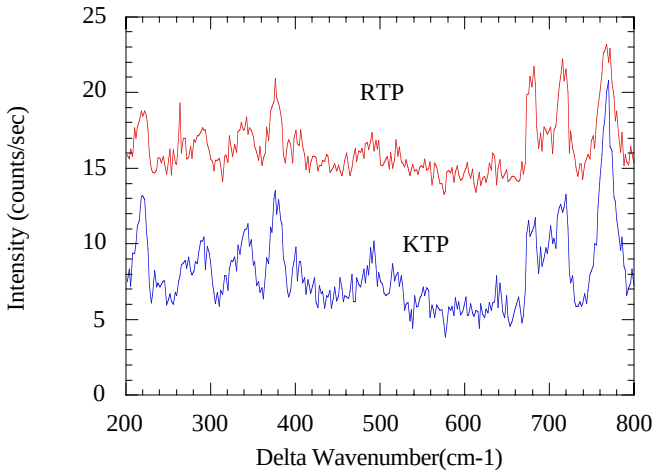

Figure 5. Near-field Raman spectra from the KTP and the RTP regions of the sample. The noise on these spectra is 1.1 counts/sec.

stretching modes (600 - 850 cm^{-1}). The Ratios between this peak and other peaks in the spectra indicate that the 767 cm^{-1} peak is almost twice as high in the RTP region as in the bulk region. While scanning the sample with the spectrometer tuned to this wavenumber, one would expect to see a higher Raman intensity in the RTP regions. Figure 6 a) shows such a scan. It is a 4μm square Raman image of the lower right hand corner of a Rb doped region similar to the one shown in figure 4. The vertical range in the Raman image is from 675 counts to 965 counts with a background noise of 32 counts. Figure 6 b) is a transmission image of the same area. Contrast is observed due to changes in the refractive index and the absorption coefficient between the Rb doped region and the KTP region. The relative light intensity in the transmission image ranges from 0.79 to 1.00 with a background noise of 0.03 in arbitrary units. The Raman image took over ten hours to complete, and is the first near-field image obtained in a Raman spectral line. The sample drift rate is 3 Å/min corresponding to a 200 nm drift over the entire duration of the scan. The probe aperture size is estimated to be slightly smaller than 1/4 micron, which is consistent with other near-field spectroscopic studies[14].

The small Raman signal levels and consequent long integration times limit measurement possibilities. However, system improvements should significantly

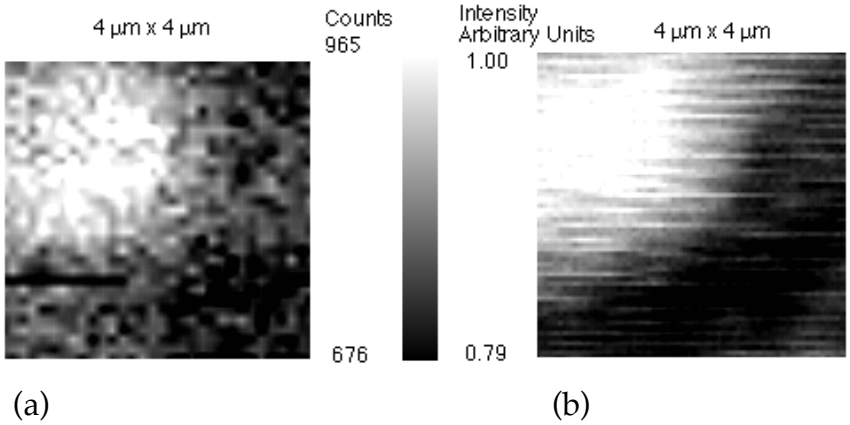

Figure 6. a) A 4 μm square Raman image of the lower right hand corner of a Rb-doped portion of the sample shown in figure 4. b) A transmission NSOM image of the same region.

improve the situation making the technique more generally applicable. Improvements which would speed all modes of operation include the use of detectors with increased quantum efficiency, and a more efficient spectrometer. The use of a parallel detector would greatly aid the acquisition of spectra, but would not contribute to reduced imaging times. It would, however, increase the amount of information gathered during the imaging process. An ultra-stable near-field instrument is still required.

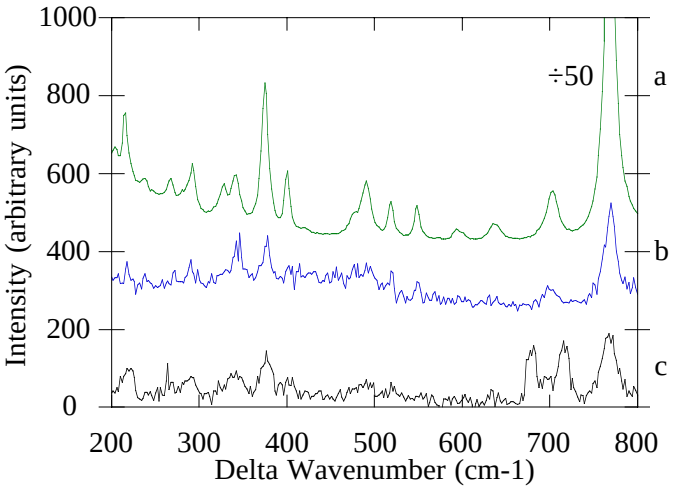

Figure 7. Three Raman spectra on KTP obtained with the same spectrometer and detector are shown. a) is a microRaman spectrum taken with a conventional optical microscope, b) is a Raman spectrum taken with the NSOM where the fiber probe is removed from the near-field region, and c) is a near-field Raman spectrum.

V. Differences Between Near-field and Far-field Measurements

To contrast the information obtained in the near-field with that from the far-field, a microRaman spectrum and a Raman spectrum taken through a fiber probe not in the near-field are shown with the near-field spectrum in figure 7. The micro Raman spectrum is obtained in the same configuration as the nanoRaman. That is the spectrometer and detection system are identical in the two experiments, and both of the signals are collected in a backscattering geometry. The microRaman experiment, however, involves the use of a 40x objective with a numerical aperture of 0.65 to illuminate the sample instead of the coated tapered fiber optic probe used in the near-field and far-field fiber probe cases.

There are many differences between the near-field vs. far-field spectra shown in figure 7. We will highlight three of these features, the Rayleigh tail, polarization, and surface sensitivity. First, the Rayleigh tail in the near-field data is greatly reduced, if not eliminated, over the spectral range shown in the figure. Since Rayleigh scattering is increased by sample inhomogeneities, the reduction of this scattering observed through the probe indicates that there is a smaller sampling volume in contrast with the microRaman case, as expected. Raman scattering from the SiO_2 fiber is also vanishingly small in the near field case seen in figure 7.

In their investigation of single molecules, Betzig and Chichester examined the electric field emerging from their fiber probes[15]. Since the single dye molecule acts as a dipole moment, it was used to determine the polarization of the electric field. By comparing the square of the electric field components that are predicted to exist at a subwavelength aperture, with their near-field images of the single molecules, they were able to determine that there is a component of the electric field in the z-direction. It is the evanescent fields emerging from the aperture which result in a large z-polarization component (i.e. directed normal to the sample surface) which would not be present in the far field. To further explore the possibility that a z-polarization component could produce peaks present in our KTP spectra, we compared our data to polarized Raman spectra on KTP obtained by Yang et al[12]. Our data should not contain any peaks corresponding to the B1 or B2 vibrational modes unless there is a z-polarization component of the electric field. Table 1 contains a summary of the data obtained by Yang, and a summary of our data. The first four columns contain the Raman peaks observed by Yang et. al. for the four vibrational modes. The letters after the peaks indicate whether they are strong (s), medium (m), weak (w), very weak (vw) , or a shoulder (sh). The fifth column contains the peaks that we observed in the near field spectra. The last four columns are an attempt to assign these peaks to the various vibrational modes based on a comparison with the data from Yang et. al. One could argue that some of the near-field "peaks" are in the noise. In addition to this difficulty, in order to obtain a larger signal, we sacrificed some spectral resolution so that our resolution was 4 cm^{-1}. On the other hand, all of the near-field peaks listed in table 1 are present in more than one near-field spectrum. With these two qualifiers in mind, we submit that the near-field peaks that are listed in bold in table 1 are evidence that part of the electric field is polarized in the z-direction. The peaks in the region of 220 cm^{-1} and 378 cm^{-1} correspond to the B2 vibrational modes and should not be observed in a backscattering geometry in the z-direction.

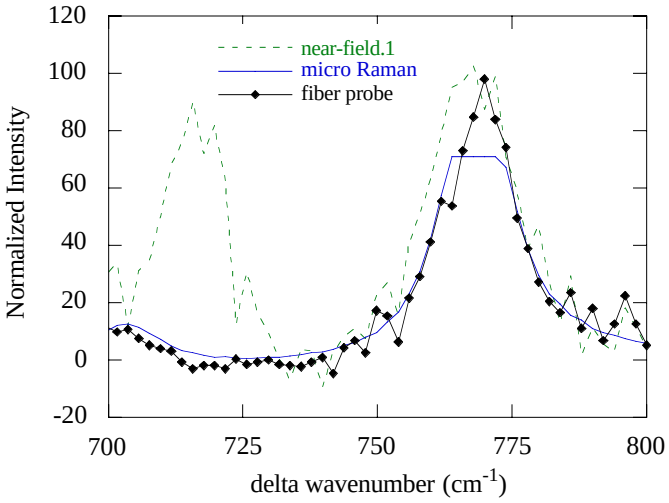

Figure 8. NanoRaman, Raman through a fiber probe removed from the near field, and microRaman spectra on KTP normalized to the peak at 767 cm^{-1}.

To compare the near-field and far-field data for these peaks, we normalized all data to the peak at 767 cm^{-1}. Figure 8 shows the normalization peak. The comparison between the data for the spectral region between 200 cm^{-1} and 300 cm^{-1} is shown in figure 9. The micro-Raman and far-field fiber probe spectra contain a peak at 215 cm^{-1}, which is an allowed A1 vibrational mode according to Yang. The near-field spectrum has a higher intensity than the micro-Raman case and is broadened and shifted towards the 220 cm^{-1} disallowed B1 vibrational mode. This is what we would expect with a z-polarization component. The intensity would be higher because more oscillators would be excited, and instead of seeing a single peak at 215 cm^{-1} and another at 220 cm^{-1}, one would expect to see a broader peak somewhere between the two, given our spectral resolution. Note also that the baseline of the near-field Raman case is lower than that of the other two far-field measurements due to the smaller Rayleigh tail. In summary, the combination of the shift and increased area under the peaks in this and the 300cm^{-1} to 400 cm^{-1} spectral regions strongly support the presence of a z-polarization component of the electric field (and hence different selection rules) at our near-field aperture. We have also shown that retraction of the probe from the surface will decrease this effect, so that the component can be identified.

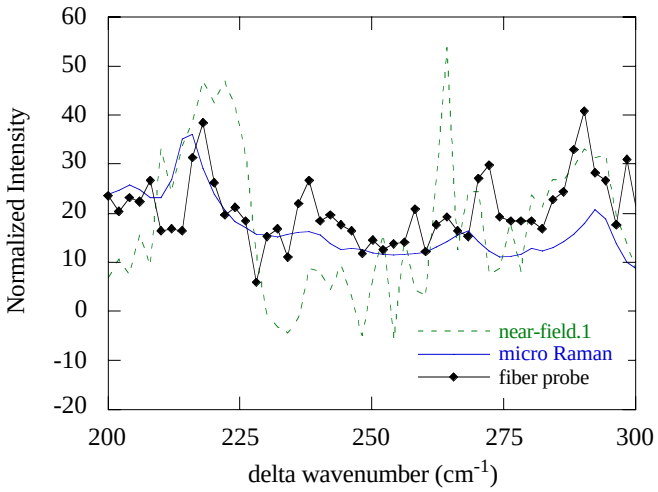

Figure 9. NanoRaman, Raman through a fiber probe removed from the near field and microRaman spectra normalized to the peak at 767 cm^{-1} highlighting the region between 200 and 300 cm^{-1} indicating the presence of a z-polarization component in the optical probe.

Author	Yang et. al.			Jahncke et. al.				
c(aa)c c(bb)b	c(ac)b	a(cb)c a(cb)a	c(ba)b c(ab)a	c(abab)c				
A1	B1	B2	A2	Raman shift	A1	B1	B2	A2
204 w	201 vw	202 s	201 w	206	206			
215 m	213 w		214 vw					
	222 w	220 s	222vw	218,222		**222**	**218**	**222**
		230 m	235 vw					
241 w	238 w			238,244	244	238		
262 w	254 m		252 m	252, 256, 264	264	256		252
269 w	268 m	268 s	268 m	269	269	269	269	269
278 m				276				
292 vw	289 s	290 m	288 m	290 vb	290	290	290	290
299 m	298 m sh	297 m						
		308 m						
320 m	316 s		318 w	318,322	322		318	
		328 vs	327 vw					
340 m	341 vw		343 s	342	342			342
	348 vw sh							
373 m	368 m	372m	372vw	366 sh				
		381 m	383 vw	378			**378**	
400m	400w	399 w		400				
	407 w	414 m	412 vw	414			414	
422 m	425m	420 m	421 vw	422	422			
431 m sh			428 vw					
443 w				446	446			
	468 w	465 m	468 vw	460			460	
475 m				476	476			
488 w	485 m	485 w	488 vw	485, 490	490	485	485	490
	499m		508 vw					
518 s	517 vw	515 vw	517 vw	513, 519	519		513	
			536 vw	531				
547 m	546 vw		546 vw					
	554 vw	554 vw		552		552	552	
570 vw	558 w	563 m	563 vw	565			565	
592 m	595 w			585, 591	591			
599 vw		597 m	600 vw					
631 m	631 w sh	639 s	641 vw	631, 637	631		637	
683 w	642 m		655 vw	681, 642	681	642		
694 w sh	699 m	701 vs	695 m	699		699	699	
			721 vw	716,				716
		730 m	731 vw					
767 vs	755 m		754 w	767	767			
	783 s	791 vw	789 m					

Table 1. Summary of Raman data from Yang et al. (1st 4 columns) and us other columns). The first 4 columns are the assignments of the peaks for the four vibrational modes. The fifth column contains the peaks we observe in the near-field spectra. The last four columns are an attempt to assign the near-field peaks to the vibrational modes identified in the first four columns.

The third feature that is of particular interest is most obvious in the spectral region around 700 cm^{-1}. Both the microRaman and the Raman data obtained with a probe in the far field show a single peak at 700 cm^{-1}. The near-field spectrum, on the other hand, has two large (or arguably three) peaks centered around 700 cm^{-1}. There are several possible explanations for the different character of the near-field spectrum, including a z-polarization effect and surface sensitivity, but the most likely explanation derives from the sensitivity of the NSOM to the surface in such a way that it can detect the change in the vibrational frequency due to nearby surface stress. Such surface sensitivity is expected since the metal coating on the probe can cause some surface enhancement[16, 17]. Let us first test the polarization hypothesis. Yang reports a peak at 683 cm^{-1}, however, it is an A1 vibrational mode and should be observed in the micro-Raman spectrum. The addition of a z-polarization should not affect its observation. The only group to report a peak at 716 cm^{-1} was Kugel et. al.[13]. They report observing this peak in the B1 geometry, so a z-polarization component would be required for its observation. However, they also report that the A1 and B2 vibrational modes are very strong compared with the A2 and B1 modes which are approximately 2% and 16% respectively of A1 or B2. This explains why there are so few near-field peaks assigned to these modes in table 1, and why the peaks which could be assigned to these vibrational modes occur for more than one mode. However, it is unlikely that a z-polarization component can fully explain our observations. According to this argument the 716 cm^{-1} peak should not be observed at all due to its lack of intensity much less appear as a strong peak.

We conclude that it is very likely that the near-field probe is providing a sensitivity to the surface resulting in the new peaks observed on either side of the peak at 700 cm^{-1}. In addition, we have presented evidence that there is a polarization component of the electric field normal to the surface being studied. This type of NSOM geometry could be used to probe Raman active vibrational modes of thin films and other materials which would be inaccessible otherwise.

VI. Summary

We have presented nano-Raman spectra of undoped and Rb-doped KTP as well as an NSOM image taken within a Raman feature. A detailed examination of the spectra suggests that the metal-coated tapered glass fiber probe grants to the NSOM an enhanced sensitivity to certain Raman features. In addition, the data show that the NSOM probe results in a polarization component of the electric field normal to the surface of the sample under investigation. The effects of this component are manifest in the Raman spectrum.

A comparison of near-field Raman spectroscopy with micro-Raman or confocal Raman spectroscopy reveals advantages and disadvantages of each technique. The primary advantages of confocal Raman spectroscopy are axial resolution and increased signal compared with near-field measurements. It is probably the better of the two for measurements far beneath a surface. The advantages of near-field Raman spectroscopy include the following. The near-field microscope can obtain sample topography and transmission images simultaneously with the Raman image. The near-field Raman data indicate a surface enhancement and a z polarization effect which could be used to obtain different information than the far-field techniques. Finally, near-field Raman is not diffraction limited so that higher resolution information can be obtained. These properties allow the near-field NSOM to localize the sampled volume in three dimensions -- to a surface. The primary disadvantage of the near-field technique is the diminished intensity of the already weak Raman signal.

Acknowledgements

We gratefully acknowledge important discussions with Boris Yakobson and Andres LaRosa. Support was provided by the US Army Research Office under grants DAAM04-94-G-0064, DAAHO4-94-G-0156 and DAAH04-93-G-0194.

References

[1] D.W. Pohl, W. Denk and M. Lanz, Applied Physics Letters **44**, 651 (1984).
[2] A. Lewis, M. Isaacson, A. Harootunian and A. Murray, Ultramicroscopy **13**, 227 (1984).
[3] E. Betzig, J.K. Trautman, T.D. Harris, J.S. Weiner and R.L. Kostelak, Science **251**, 1468 (1991).
[4] Proceedings of NFO-3, Brno, Czech Republic, Elsevier (1995).
[5] M.A. Paesler and P.J. Moyer, "Near-Field Optics," (Wiley, New York, 1995).
[6] P. Moyer, Ph.D. thesis, North Carolina State University (1993).
[7] K. Takata, T. Hasegawa, S. Hosaka, S. Hosoki and T. Komada, Applied Physics Letters **55**, 1718 (1989).
[8] C. L. Jahncke and H. D. Hallen, (manuscript in progress).
[9] John D. Bierlein and Herman Vanherzeele, Journal of the O□ptical Society of America B **6**, 622 (1989).
[10] John D. Bierlein, August Ferretti, Lothar H. Brixner and William Y Hsu, Applied Physics Letters **50**, 1216 (1987).
[11] J. D. Bierlein, D. B. Laubacher and J. B. Brown, Applied Physics Letters **56**, 1725 (1990).
[12] Hua-guang Yang, Ben-yuan Gu, Yan-yun Wang, Huang Cheng-en and De-zhong Shen, Guangxue Xuebac **6**, 1071 (1986).
[13] G. E. Kugel, F. Brehat, B. Wyncke, M. D. Fontana, G. Marnier, C. Carabatos-Nedelec and J. Mangin, Journal of Physics C: Solid State Physics **21**, 5565 (1988).

[14] R. D. Grober, T. D. Harris, J. K. Trautman, E. Betzig, W. Wegscheider, □L. Pfeiffer and K. West, Appl. Phys. Lett. **64**, 1421 (1994).
[15] Eric Betzig and Robert J. Chichester, Science **262**, 1422 (1993).
[16] L. Novotny, D.W. Pohl and P. Regli, Journal of the Optical Society of America, A. **11**, 1768 (1994).
[17] D.A. Christensen, Ultramicroscopy **57**, 189 (1995).